L-H TRANSITION STUDIES AT JET: TRITIUM, HELIUM AND DEUTERIUM.

E. R. SOLANO
Laboratorio Nacional de Fusion, CIEMAT
Madrid, SPAIN
Email: emilia.solano@ciemat.es

The JET L-H transition team* and JET Contributors **

* See Appendix A at the end
** See the author list of 'Overview of JET results for optimising ITER operation' by J. Mailloux et al to be published in Nuclear Fusion Special issue: Overview and Summary Papers from the 28th Fusion Energy Conference (Nice, France, 10-15 May 2021)

Abstract

We present an overview of results from a series of L-H transition experiments undertaken at JET since the installation of the ITER-like-wall (JET-ILW), with Beryllium wall tiles and a Tungsten divertor. Tritium Helium and Deuterium plasmas have been investigated. Initial results in RF-heated Tritium show an unexpectedly high threshold when compared to Deuterium, to be investigated further. In Helium plasmas there is a notable shift of the density at which the power threshold is minimum ($n_{e,min}$) to higher values relative to Deuterium and Hydrogen references, and a drop in threshold at high densities. Transport modelling in slab geometry shows that in Helium neoclassical transport competes with interchange-driven transport, unlike in Hydrogenic isotopes. Measurements of the radial electric field in Deuterium plasmas show that E_r shear is not a good indicator of proximity to the L-H transition. Transport analysis of ion heat flux in Deuterium plasmas show a non-linearity as density is decreased below $n_{e,min}$. Lastly, a regression of the JET-ILW deuterium data is compared to the 2008 ITPA scaling law.

1. INTRODUCTION

Characterizing and understanding the power threshold conditions for ITER to achieve H-modes (P_{LH}) is a major goal of a series of L-H transition experiments undertaken at JET since the installation of the ITER-like-wall (JET-ILW), with Beryllium wall tiles and Tungsten divertor [1-4]. In this contribution we report on results from L-H transitions studies in Tritium, ^{4}Helium and Deuterium plasmas.

All L-H transition experiments presented here are carried out with slow power ramps, ~1 MW/s. The effect of strike line location on the L-H power threshold is very strong in JET-ILW [1]. All plasmas discussed in detail in this manuscript have the same shape, HT shown in Fig. 1c, with the inner strike line on the vertical target and the outer strike line on a tilted target. Other shapes shown in Fig. 1 will be discussed later. The L-H transition power threshold, P_{LH}, is measured either as $P_{loss} = P_{Ohm} + P_{Aux} - dW/dt$ or as $P_{sep} = P_{loss} - P_{rad,bulk}$

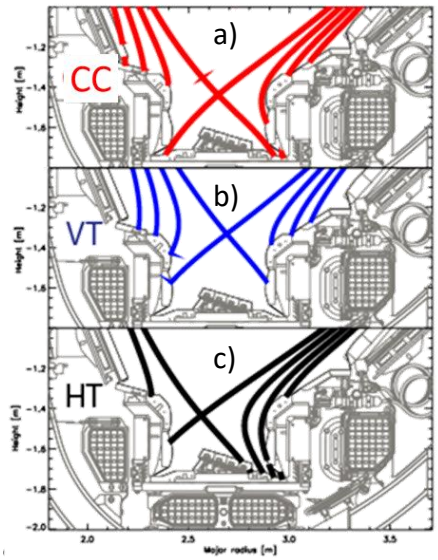

Fig. 1: typical plasma shapes at JET: a) CC, Corner, b) VT, Vertical Target and c) HT, Horizontal Target.

2. L-H TRANSITION STUDIES IN TRITIUM PLASMAS

While waiting for the Neutral Beam Injection (NBI) system change-over from Deuterium (D) to Tritium (T), and after a few Hydrogen (Protium, H) and H+T experiments, we had the opportunity to investigate L-H transitions in Tritium plasmas with RF ion cyclotron resonant heating with H minority (n_H/n_e~5%). The L-H transition studies in Tritium presented here were performed in plasmas with B_{tor}=1.8 T, I_p=1.7 MA, HT shape.

Shown in Fig. 2a is the typical behaviour observed: during the RF power ramp, the plasma enters the H mode briefly: edge density rises, divertor D_α drops, radiation rises and a back-transition follows. In this case, after 4 dithers the plasma stays in H-mode.

Previous L-H transition studies in JET with a Carbon wall and a similar shape and divertor [5] led us to expect that $P_{LH}(T)<P_{LH}(D)$. Alas, this is not the case in JET-ILW: we could barely reach H-mode in Tritium L-H

transition experiments, and when H-mode was reached the electron temperature at the pedestal, $T_{e,ped}$, remained cold, <100 eV. A matching Deuterium pulse with similar n_e, P_{sep} had $T_{e,ped}$ ~200 eV.

The dithering power threshold is displayed in Fig. 3a: P_{sep} values that do induce L-H transitions in D, lead to at most transient H-modes in T. The dithers are marked with magenta "+" signs. Only 1 steady transition was obtained, the magenta diamond. Note that bulk radiation, plotted in Fig. 3b, is much larger in Tritium than in Deuterium. Even the ohmic and quasi-ohmic Tritium transitions observed at low densities exhibit higher radiation than comparable heated Deuterium plasmas, as shown in Fig. 3b. The enhanced radiation in Tritium may well be due to enhanced Be production by Tritium that leads to increased sputtering of the W divertor, but transport may also play an additional role. Detailed investigation of the dynamics of these transient H-modes is underway, and further experiments are planned.

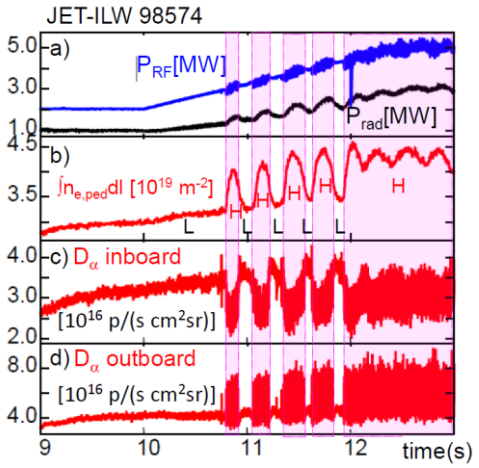

Fig. 2: L-H transitions in Tritium: a) Input RF power and bulk radiation; b) line-integrated pedestal density; c) D_α from inboard divertor; d) D_α outboard divertor

Measurements of H, D, and T concentration in the JET sub-divertor region are available from an Optical Penning Gauge [6,7]. In all cases reported here n_T/n_{H+D+T}>95%.

In these pulses **no** Deuterium was injected, but trace concentrations of residual Deuterium were present. Using a combination of TRANSP modelling [8] and neutron measurements we find that n_D/n_e<1%, with about 75 % of neutrons being produced by the T(T,2n)^{4}He reaction, the remainder stemming from DT fusion [9].

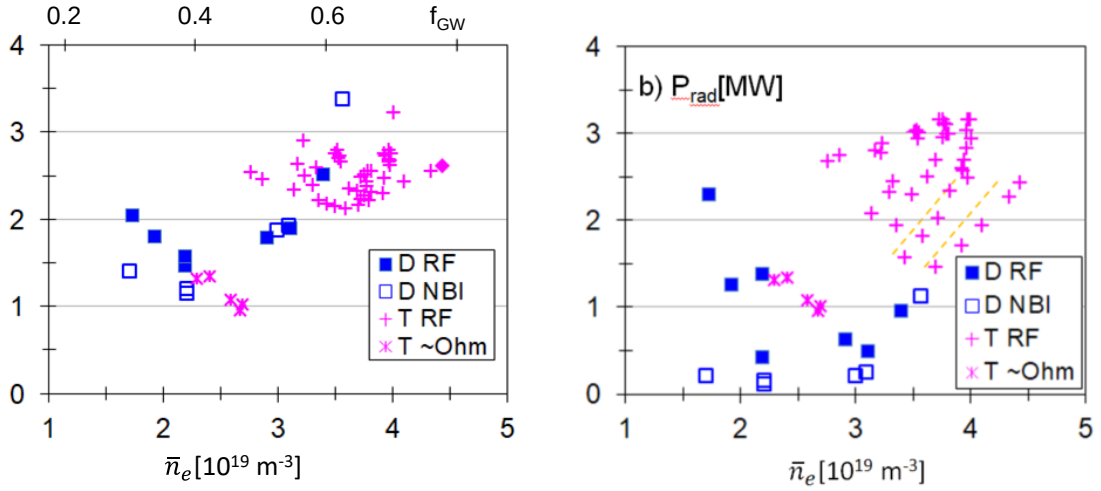

*Fig. 3a: $P_{sep}(n_e)$ for Deuterium (blue squares) and Tritium. In **Tritium** most transitions were dithers, marked with a +. The only true L-H transition in Tritium is the diamond at high density.*
Fig. 3b: Bulk radiation (inside PSIN=0.95).

3. L-H TRANSITION AND ELM STUDIES IN HELIUM PLASMAS

The ITER Research Plan includes a Pre-Fusion Operation Power (PFPO) phase with either Hydrogen or Helium plasmas in order to study ELMy H-modes at low toroidal field as early as possible, before the nuclear phase that starts with Deuterium plasmas. We studied the L-H power threshold in ^{4}Helium plasmas in the JET-ILW to compare with Hydrogen and Deuterium plasmas.

To ensure minimal contamination of the Helium plasmas in this study, we took advantage of 18 calibration pulses taken with only Helium gas injection (no injection of Hydrogenic species). These pulses, unrelated to our experiments, ensured Helium purity: they had Z_{eff}=2±0.05. Throughout the calibration pulses and the L-H transition pulses, the divertor cryopump operated as usual, removing hydrogenic species. No Argon frosting was used to pump Helium. For RF heating the H concentration n_H/n_e was kept below 5%. Spectroscopic measurements of ^{4}He concentration show that in all cases the L-H transition happens with Helium concentration n_{He}/n_e> 0.48, and corresponding Helium fraction $n_{He}/(n_{He}+n_H+n_D)$> 0.92.

3.1. L-H transition power threshold in He, H, D

For ITER it is important to predict the L-H transition power threshold in Hydrogen and Helium plasmas to determine the operational space of such plasmas in PFPO. Such a prediction was made inspired by the AUG observation that in an electron heated plasma a sufficient edge ion heat flux is necessary to achieve a sufficient radial electric field (shear) [10]. Assuming pure electron heating in ITER, $n_{e,min}$ has been evaluated based on 1.5-D transport modelling as the density at which the ratio of edge ion power flux to total edge power flux starts to saturate with increasing electron density (line-averaged). The result of this modelling is that $n_{e,min}$~0.4 $n_{e,GW}$ for q_{95}= 3 and is weakly independent of the ion species, (H or He) [11]. The transition condition in that model is itself based on the assumption that the Helium power threshold, P_{LH}(He), is 1.4×P_{LH}(D), while P_{LH}(H)=2×P_{LH}(D), based in part on JET-C L-H transition studies [12].

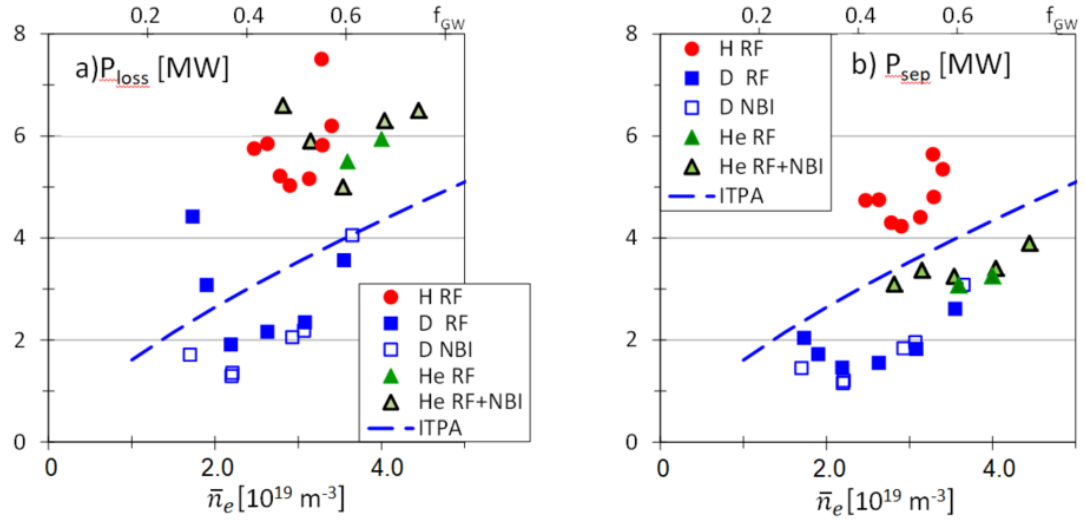

Fig. 4a) P_{loss} at the L-H transition as a function of $n_{e,av}$ (lower horizontal axis) and f_{GW} (upper horizontal axis) for Hydrogen, Deuterium and Helium HT plasmas. The dark Helium symbols correspond to pure ICRH, lighter ones with black boundary have added NBI blips. Dashed blue line indicates 2008 ITPA Deuterium scaling[3].
Fig. 4b) Corresponding P_{sep}=P_{loss}–P_{rad} plot.

The ICRH (H minority heating) power ramps were augmented by D-NBI blips, both to increase the total auxiliary power and to measure T_i. Shown in Fig. 4a is P_{loss} at the L-H transition as a function of density for Hydrogen, Deuterium and Helium in 1.8 T, 1.7 MA HT plasmas. The Helium data points in dark green reflect pure RF heating, while those with black outline correspond to transitions during the NBI blip. The transitions during the NBI blip are necessarily brief, and more power may be necessary for a transition to steady H-mode. The density at which P_{LH} is minimum, $n_{e,min}$, is considerably higher for Helium than for Deuterium, and somewhat higher than for Hydrogen. In terms of Greenwald fraction, $n_{e,min}$(D)~0.4×f_{GW}, $n_{e,min}$(H)~0.5×f_{GW}, $n_{e,min}$(^{4}He)~0.6×f_{GW}. The shift in $n_{e,min}$ is clearer in P_{loss}, Fig. 4a, but can still be seen in P_{sep}, Fig. 4b. We have found the same shift in $n_{e,min}$ with a different plasma shape (Corner, CC, see Fig. 1)) at the same field and current, and at a higher field, with NBI heating [13]. In all Helium plasmas we find that the L-H transition takes place when the outer strike line is attached, even at the highest densities. At the inner strike line the plasma is partially detached.

Radiation is notably higher for the dominantly RF-heated Helium plasmas at low density, so the auxiliary power required for the L-H transition to take place is lower for Hydrogen than for Helium below 3.3×10^{19} e/m^3. As shown in Fig. 3b, above $n_{e,min}$(He), Deuterium and Helium have similar P_{sep}, below the ITPA 2008 scaling [14]. At high density Hydrogen has much higher P_{loss} and P_{sep}: L-H transitions can't be obtained with the available RF heating. In contrast with our results, DIII-D found a ~30% increase in $n_{e,min}$(He) relative to $n_{e,min}$(D) [15], lower than the 50% change we found. AUG studies show no difference in $n_{e,min}$ between H, D and He, and the same P_{LH} for D and He [16]. C-Mod L-H transition data [17] show Helium points in the low n_e branch for n_e<0.3 n_{GW}, while in Deuterium P_{LH} increases with density, so no shift on $n_{e,min}$ could be documented.

The potential increase in the predicted P_{sep} for ITER due to higher $n_{e,min}$ in He compared to H and D is compensated by the lower power required to access it, since we recall that ITER had assumed P_{LH}(He)=1.4 P_{LH}(D), while our experiments find P_{LH}(He)=P_{LH}(D) above this density. This will be the case provided radiation won't be significantly higher in Helium plasmas compared to H plasmas in ITER.

3.2. Helium simulations with HESEL

The HESEL code [18, 19] was applied to investigate the L-H transition in a pure Helium plasma JET#93870 with an L-H transition at 15.45 s and $n_{e,av}$=4 10^{19} m^{-3}, comparing it with a Deuterium pulse of similar high density. HESEL is a four-field (Vorticity, Density, Ion, and Electron pressure), energy-conserving, drift-fluid model based on the Braginskii equations, describing interchange-driven, low-frequency turbulence in a plane perpendicular to the magnetic field at the outboard mid-plane of a Tokamak plasma. It includes the transition from the confined region to the SOL and the full development of the profiles across the LCFS. Experimental parameters and edge profiles of electron temperature and electron density just before the LH transition are used as the initial condition. The energy input to the ions is modelled by artificially increasing the ion temperature at the inner boundary of the computational domain throughout the simulation. A plasma of doubly ionized ^{4}He has $n_i=n_e/2$, so greater T_i is needed to reach a comparable ∇p_i to triggers a transition. The resulting evolution, displayed in Fig. 5, finds a transition from an L-mode to H-mode-like confinement - for $T_i \sim 3\times T_e$ at the LCFS - with significantly reduced turbulent transport of energy across the last closed flux surface. The power threshold was in the same range as the one for a similar Deuterium plasma corresponding to JET#90993, with $T_i \sim 1.5\ T_e$ at LCFS [20]. The collisional transport ($\propto Z^2$) for the Helium case is not negligible as compared with the turbulent transport, as was the case for Hydrogen isotopes [20], especially after the transition. On the other hand, we observe that the shearing rates of the zonal flow - giving rise to the edge transport barrier sustaining the H-mode - are similar for the Deuterium and Helium cases.

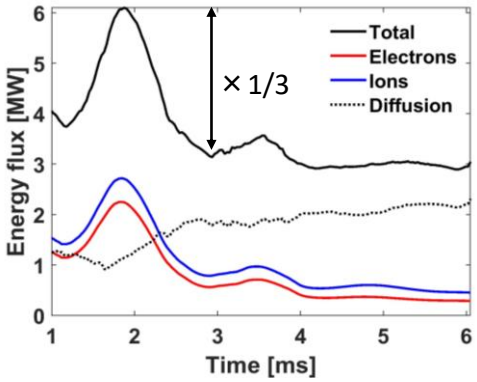

Fig. 5: Energy flux across separatrix as a function of time

3.3. ELMs in Helium plasmas

In Hydrogen and Deuterium plasmas, with sufficient NBI heating, it is common to observe the coherent M-mode [21] at the L-H transition. As input power increases small ELMs appear mixed with the M-mode, until eventually isolated ELMs appear, often described as Type I ELMs. The same pattern is observed in Helium plasmas, as shown in Fig. 6. It was not possible to document an increase in ELM frequency as power increases. Still, we find that the magnetic signals show quiet periods during the isolated ELMs, a criterion that can be used to characterise them as type I. The high ELM frequency, of order 100 Hz, and low $T_{e,ped}$<0.5 keV, imply that ELM pacing techniques such as kicks or pellets can't be tested in these Helium plasmas.

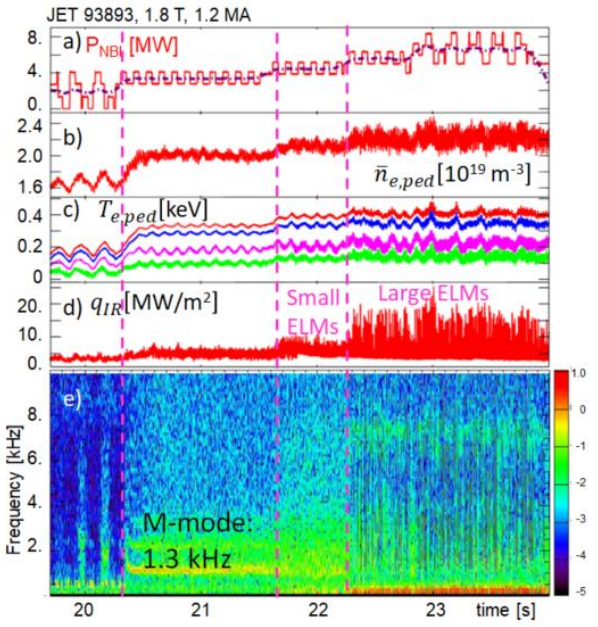

Fig. 6: ELMs in Helium D-NBI heated plasma. a) NBI input power, measured and smoothed; b) $n_{e,ped}$; c) $T_{e,ped}$; d)IR-measure heat flux at outer target; e) spectrogram of inboard Mirnov signal (log scale colour contours), showing M-mode and quiet periods in between ELMs

The estimated drop in plasma electron energy lost per ELM is 30-40 kJ, compared to 130 kJ electron pedestal energy. This high, but comparable to similar ELMs in Deuterium. An MHD stability analysis, assuming $T_i=T_e$, finds **stable** conditions just before the ELM, as is usual in high density plasmas in JET-ILW [22, 23].

The P_{sep} required to reach these type I ELMs in Helium is of order 4-5.5 MW, of order 2-2.5× the transition value, which was 2.2 MW.

4. L-H TRANSITION STUDIES IN DEUTERIUM

4.1. Evolution of edge radial electric field along power ramp

Measurements of the propagation velocity of edge fluctuations, $v_\perp = v_{E\times B} + v_{phase}$, are obtained with Doppler Reflectometry [24,25]. Typically in the edge v_{phase} is ignorable. To localise the measurement, accurate electron density profiles are necessary. The density profiles from the profile reflectometer [26] were calculated from the time-of-flight, extracted from spectrograms stacked from 10 probing frequency sweeps [27].

A detailed study of the pre-transition E_r profiles across electron density scans in Deuterium and Helium is presented in [28]. The results are qualitatively similar in Deuterium and Helium.

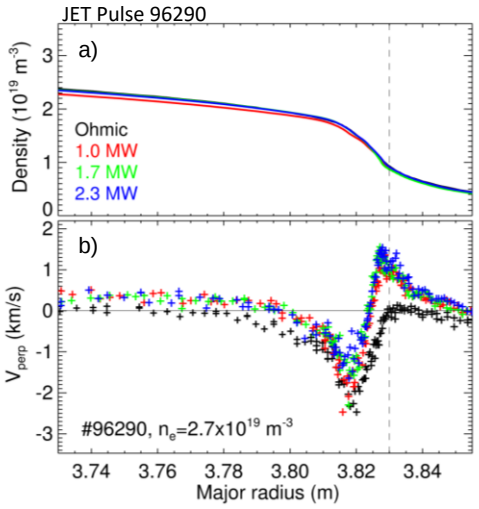

Fig. 7: Radial profiles of a) density and b) $v_\perp$ for Deuterium plasmas at different ICRH power levels ($\bar{n}_e$= 2.7×10^{19} m^{-3}). Dashed line marks separatrix.

In Fig. 7 we present electron density and $v_\perp$ profiles taken along a heating ramp used to induce the L–H transition in a Deuterium plasma in the low density branch. The SOL flow is observed to increase when the auxiliary heating is applied, but then exhibits no variation with ICRH power up to the transition, which takes place when a further 0.2 MW of heating is applied. Interestingly, no significant increase of maximum $v_\perp$ shear is observed preceding the L–H transition at the various ICRH power steps. This may suggest that the H-mode access is not only established by the mean E_r profile.

4.2. Ion heat flux analysis near $n_{e,min}$: 3 T, 2.5 MA

L-H transitions in Deuterium plasmas at high field, 3 T, 2.5 MA, were obtained to optimise threshold measurements. NBI heating was used to obtain ion temperature (T_i) measurements of the main ion species [29], to ensure the power threshold was not modified by injected impurities, which are usually needed for CX measurements in JET-ILW [30]. Experimental profiles of density and temperatures were used to calculate heating deposition profiles and fast ion losses.

A detailed transport analysis was carried out for a set of JET-ILW NBI-heated, Deuterium plasma discharges, with B_{tor}=3T, I_p=2.5 MA, to understand the relationship between the edge ion heat flux at the L-H transition and $n_{e,min}$ [31].

In all cases we found experimentally that $T_e > T_i$ in the plasma core. Although direct NBI ion heating and significant electron to ion exchange power resulted in a larger power coupled to plasma ions than to electrons, ion energy transport is shown to be dominant by gyrokinetic transport simulations, explaining the observed core $T_e > T_i$. Like the power threshold, P_{loss} or P_{sep}, the edge ion heat flux at the L-H transition exhibits non-monotonic behaviour as a function of density, as shown in Fig. 8 for a set of discharges in the $n_{e,min}$ region. A linear trend of the critical edge ion heat flux has been noted in RF-heated AUG and C-mod discharges [32], while NBI pulses both for JET [31] and AUG [16] deviate from linearity, possibly due to the role of NBI induced toroidal rotation.

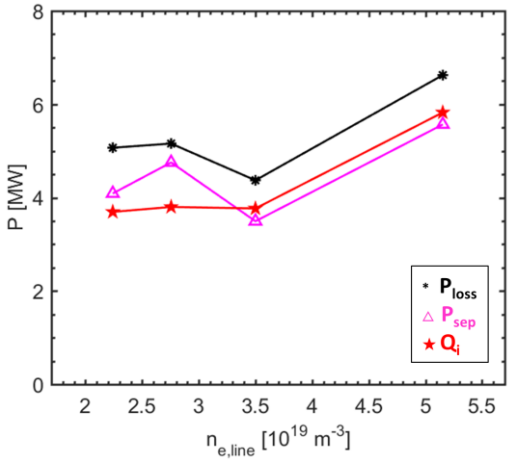

Fig. 8: Power terms at the L-H transition for a set of JET-ILW Deuterium, NBI-heated pulses. P_{loss} is shown with black asterisks, P_{sep} with magenta triangles, edge ion heat flux Qi with red stars

4.3. L-H transition scaling laws in Deuterium

A database of L-H transitions in Deuterium in the JET-ILW has been assembled as part of the ITPA TC-26 [33]. It contains 107 L-H transitions in a variety of plasma shapes, currents and fields.

Table I lists the $n_{e,min}$ values of each dataset/shape. HT-R and HT-L are versions of the HT shape (see Fig. 1) with the outer strike line shifted outward and inward relative to HT, respectively. Only data above the densities quoted on the table was fitted for each plasma configuration. The various shapes and their impact on P_{LH} were described in [1, 2, 3].

The ITPA 2008 scaling law [14] is the starting point. The conventional fitting variables are the line averaged density in units of $10^{20}m^{-3}$, n_{e20}, the toroidal field B_T and the plasma surface area S

$$P_{LH}=(0.0488\pm0.006)\, n_{e20}^{0.717\pm0.035}\, B_T^{0.803\pm0.032}\, S^{0.941\pm0.019} \qquad (4.1)$$

Table I

B_{tor} (T)	I_p(MA)	Shape	$n_{e,min}$
1.8	1.7	HT	2.2±0.3
1.8	1.7	HT	2.2±0.3
2.4	2.0	HT	2.85±0.1
2.4	2.0	HT-L	2.7±0.2
2.4	2.0	VT	< 2.0
2.4	1.5	HT-high δ	2.2±0.1
3.0	2.75	HT-R	3.3±0.2
3.0	2.5	VT	2.3±0.2
3-3.4	various	CC	2.5±0.2

Table I: $n_{e,min}$ as a function of B_t, I_p and shape in the JET-ILW Deuterium database

Fig. 9a displays the new data vs. the ITPA 2008 scaling law, showing the clear impact of shape on the power threshold.

A fit with a similar functional form, but assuming S^1, is sought for P_{loss} in the high density branch. It is found that the data naturally falls in one of two branches: the power threshold is lower for the HT configurations, with the outer strike line on the tilted target, and higher for VT and CC, when the strike lines hit vertical targets or the corners of the divertor. It is possible to develop separate scaling laws for each combined dataset:

$$P_{L-H}(HT) = (0.057\pm0.012)\, n_{e20}^{1.43\pm0.10}\, B_T^{0.77\pm0.015}\, S^1, \qquad RMSE=17\% \qquad (4.2)$$

$$P_{L-H}(VT/CC) = (0.031\pm0.013)\, n_{e20}^{0.77\pm0.20}\, B_T^{1.29\pm0.24}\, S^1, \qquad RMSE=10\% \qquad (4.3)$$

Here we note that the sum of density and field coefficients is similar in both cases, with stronger density dependence for the HT shape. Combining both datasets with a simple factor to account for the difference in power threshold due to plasma shape, we obtain a single scaling law with hardly any change of relative RMSE:

$$P_{L-H}= D\,(0.046\pm0.009)\, n_{e20}^{1.31\pm0.09}\, B_T^{0.85\pm0.13}\, S^1, \qquad RMSE=16\% \qquad (4.4)$$

with D=1.0 for HT,HT-R and HT-L and D=2.06 +/- 0.07 for VT/CC

This scaling law is plotted in Fig. 9 b. The density scaling coefficient has increased relative to ITPA 2008.

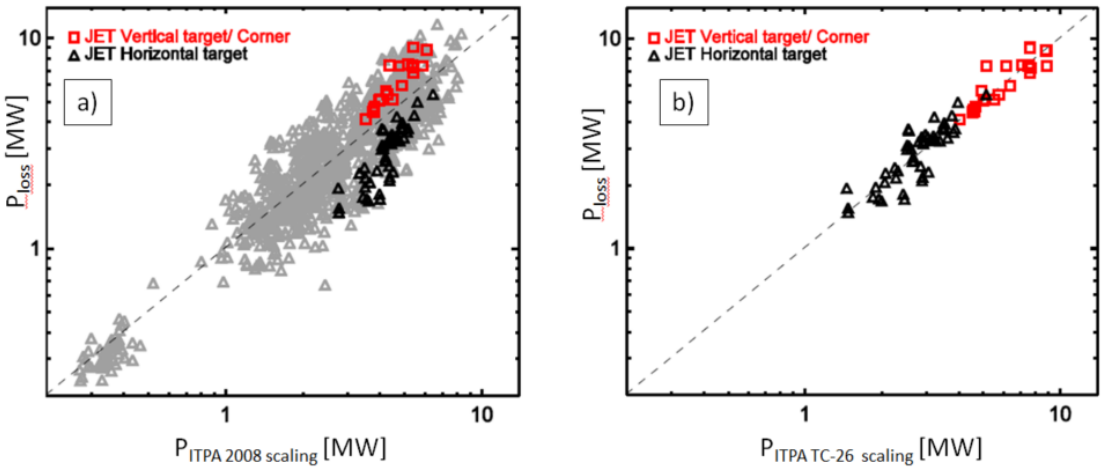

Fig 9a): P_{loss} data vs ITPA 2008 scaling, equation (4.1), 9b) P_{loss} data vs TC-26 2017 scaling, equation (4.4).

5. SUMMARY AND OUTLOOK

Recent L-H transition studies at JET have obtained novel results for the dependence of the L-H transition power threshold on ion species.

A surprising high L-H transition threshold was observed in RF heated Tritium L-H transition experiments. Increased bulk radiation can't fully explain it. Further experiments are planned with NBI heating and at different fields, to establish if this observation is related to RF heating.

The Helium power threshold results are ambiguous for ITER prediction: access to H-mode in the PFPO phase of the ITER Research Plan may only be easier in Helium than in Hydrogen at higher densities. Still, the He H-mode threshold power itself is comparable to D and, not 40% higher as previously assumed, compensating the increase in required power to access the H-mode in Helium at higher densities. Modelling shows that heat transport is quite different in Helium plasmas, with a large collisional contribution both in L and H-mode. And type I ELMs can be obtained in Helium with NBI heating.

Novel Doppler reflectometry measurements in RF-heated Deuterium plasmas challenge the assumption that the radial electric field shear builds up along the power ramp, until a critical value triggers the transition.

Detailed transport analysis of the ion heat flux in Deuterium NBI heated plasmas near $n_{e,min}$ finds that it departs from a linear dependency in n_e as density decreases.

Scaling laws for the L-H transition power threshold in the JET-ILW (restricted to the high density branch) have been derived, accounting for shape dependency.

Together this set of results advance understanding of the L-H transition and improve the predictive capability towards operation in ITER and future tokamaks.

ACKNOWLEDGEMENTS

This work has been carried out within the framework of the EUROfusion Consortium and has received funding from the Euratom research and training programme 2014-2018 and 2019-2020 under grant agreement No 633053. The views and opinions expressed herein do not necessarily reflect those of the European Commission or the ITER organization. Additionally, work is supported in part by the Spanish National Plan for Scientific and Technical Research and Innovation 2017-2021, grant number FIS2017-85252-R

REFERENCES

[1] CF Maggi et al 2014 Nucl. Fusion 54 023007,
[2] E Delabie, Proc. of the 25th IAEA Fusion Energy Conference, Saint Petersburg, Russia, EX/P5 (2014)
[3] J Hillesheim et al Proc. of the 26th IAEA FEC, Kyoto, Japan, (2016)
[4] J Hillesheim et al Proc. of the 27th IAEA FEC, Gandhinagar, India (2018)
[5] E Righi et al 1999 Nucl. Fusion 39 309
[6] U.Kruezi et al 2020 JINST 15 C01032
[7] S Vartanian, E Delabie, CC Klepper, et al, Fusion Engineering and Design, Vol. 170, p. 112511 (2021)
[8] J.P.H.E. Ongena, Fusion Science and Technology; v. 45; p. 371-379, 2012
[9] Z. Štancar, to be presented at EPS 2021
[10] F Ryter et al 2013 Nucl. Fusion 53 113003
[11] ITER Research Plan within Staged Approach, ITR-Report 18-003 (2018) p 351
[12] D McDonald et al, *Plasma Phys. Control. Fusion* 46 519 (2004)
[13] E. R. Solano, to be submitted to NF
[14] Y. Martin, et al 2008 J. Phys.: Conf. Ser. 123 012033
[15] P. Gohil et al, Nucl. Fusion 51 (2011) 10
[16] F Ryter et al, Nucl. Fusion 54 083003 (2014)
[17] C.E. Kessel et al 2018 Nucl. Fusion 58 056007
[18] J. Juul Rasmussen et al., (2016), Plasma Phys. Contr. Fusion, 58, 014031
[19] A.H. Nielsen et al., (2015), Physics Letters A, 379, 3097
[20] A.H. Nielsen et al. Invited talk, 29th International Toki Conference on Plasma and Fusion Research, Japan, 2020
[21] ER Solano et al, Nuclear Fusion, 57, 022021 (2017)
[22] CF Maggi Nucl. Fusion 55 (2015) 113031
[23] L Frassinetti, this conference, EX/2-1050 and P3-1445
[24] J.C. Hillesheim et al., Proc. 12th Inter. Reflectometry Workshop, IRW12

[25] C. Silva et al., Nucl. Fusion 56 (2016) 106026
[26] A. Sirinelli et al., Review of Scientific Instruments 81, 10D939 (2010)
[27] P. Varela et al, Nucl. Fusion 46 S693 (2006)
[28] C. Silva, to be submitted to Nucl. Fusion.
[29] E. Delabie et al, 23rd Topical Conference on High-Temperature Plasma Diagnostics, Santa Fe, United States, May 2020
[30] S. Menmuir et al., Review of Scientific Instruments 85, 11E412 (2014)
[31] P. Vincenzi et al., 46th EPS Conf.on Plasma Physics, P2.1081, Milano, Italy (2019), to be submitted to Nuclear Fusion
[32] M. Schmidtmayr et al 2018 Nucl. Fusion 58 056003]
[33] E. Delabie et al, 'Status of TC-26: L-H/H-L scaling in the presence of Metallic walls', ITPA meeting September 2017

Appendix A: the JET L-H transition team

E.R. Solano[1], E. Delabie[2], G. Birkenmeier[3,4], C. Silva[5], J. Hillesheim[6], P. Vincenzi[7], A.H. Nielsen[8], J.J.ºRasmussen[8], A. Baciero[1], S. Aleiferis[6,9], I. Balboa[6], A. Boboc[6], C. Bourdelle[10], I.S. Carvalho[5], P. Carvalho[5], M.ºChernyshova[11], R. Coelho[5], T. Craciunescu[12], R. Dumont[10], E. de la Luna[1], J. Flanagan[6], M. Fontana[13], J.M.ºFontdecaba[1], L. Frassinetti[14], D. Gallart[15], J. Garcia[10], E. Giovannozzi[16], C. Giroud[6], W.Gromelski[11], R.Henriques[5], L. Horvath[6], I. Jepu[12], A. Kappatou[4], D.L. Keeling[6], D. King[6], E. Kowalska-Strzęciwilk[11], M.Lennholm[17], E. Lerche[18], E. Litherland-Smith[6], V. Kiptily[6], K. Kirov[6], A. Loarte[19], B. Lomanowski[20], C.F.ºMaggi[6], M.J. Mantsinen[21], A. Manzanares[22], M. Maslov[6], A.G. Meigs[6], R.B. Morales[6], D. Nina[5], C.ºNoble[6], V. Parail[6], F. Parra Diaz[23], E. Pawelec[24], G. Pucella[16], D. Réfy[25], E. Righi-Steele[17], F.G. Rimini[6], T.ºRobinson[6], S. Saarelma[6], M. Sertoli[6], A. Shaw[6], S. Silburn[6], P. Sirén[6], Z. Stancar[26], H. Sun[6], G. Szepesi[6], D. Taylor[6], E.ºTholerus[14], S.ºVartanian[10], G. Verdoolaege[27], B. Viola[16], H. Weisen[13] and T. Wilson[6]

[1]Laboratorio Nacional de Fusión, CIEMAT, Madrid, Spain; [2]Oak Ridge National Laboratory, Oak Ridge, TN 37831-6169, TN, United States of America; [3]Physik-Department E28, Technische Universität München, 85748 Garching, Germany; [4]Max-Planck-Institut für Plasmaphysik, D-85748 Garching, Germany; [5]Instituto de Plasmas e Fusão Nuclear, Instituto Superior Técnico, Universidade de Lisboa, Portugal; [6]CCFE, Culham Science Centre, Abingdon, Oxon, OX14 3DB, United Kingdom of Great Britain and Northern Ireland; [7]Consorzio RFX, Corso Stati Uniti 4, 35127 Padova, Italy; [8]Department of Physics, Technical University of Denmark, Bldg 309, DK-2800 Kgs Lyngby, Denmark; [9]NCSR 'Demokritos' 153 10, Agia Paraskevi Attikis, Greece; [10]CEA, IRFM, F-13108 Saint Paul Lez Durance, France; [11]Institute of Plasma Physics and Laser Microfusion, Hery 23, 01-497 Warsaw, Poland; [12]The National Institute for Laser, Plasma and Radiation Physics, Magurele-Bucharest, Romania; [13]Ecole Polytechnique Fédérale de Lausanne (EPFL), Swiss Plasma Center (SPC), CH-1015 Lausanne, Switzerland; [14]Fusion Plasma Physics, EES, KTH, SE-10044 Stockholm, Sweden; [15]Barcelona Supercomputing Center, Barcelona, Spain; [16]Unità Tecnica Fusione, ENEA C. R. Frascati, via E. Fermi 45, 00044 Frascati (Roma), Italy; [17]European Commission, B-1049 Brussels, Belgium; [18]Laboratory for Plasma Physics Koninklijke Militaire School, Ecole Royale Militaire Renaissancelaan 30 Avenue de la Renaissance B-1000, Brussels, Belgium; [19]ITER Organization, Route de Vinon, CS 90 046, 13067 Saint Paul Lez Durance, France; [20]Aalto University, PO Box 14100, FIN-00076 Aalto, Finland; [21]ICREA and Barcelona Supercomputing Center, Barcelona, Spain; [22]Universidad Complutense de Madrid, Madrid, Spain; [23]Rudolf Peierls Centre for Theoretical Physics, University of Oxford, Oxford OX1 3PU, United Kingdom of Great Britain and Northern Ireland; [24]Institute of Physics, Opole University, Oleska 48, 45-052 Opole, Poland; [25]Wigner Research Centre for Physics, POB 49, H-1525 Budapest, Hungary; [26]Slovenian Fusion Association (SFA), Jozef Stefan Institute, Jamova 39, SI-1000 Ljubljana, Slovenia; [27]Department of Applied Physics, UG (Ghent University), St-Pietersnieuwstraat 41 B-9000 Ghent, Belgium;